Raman Characterization of ABA- and ABC-Stacked Trilayer Graphene

Chunxiao Cong,[†] Ting Yu,[†,‡,*] Kentaro Sato,[§] Jingzhi Shang,[†] Riichiro Saito,[§] Gene F. Dresselhaus,[⊥] and Mildred S. Dresselhaus[¶,#]

[†]Division of Physics and Applied Physics, School of Physical and Mathematical Sciences, Nanyang Technological University, 637371, Singapore, [‡]Department of Physics, Faculty of Science, National University of Singapore, 117542, Singapore, [§]Department of Physics, Tohoku University, Sendai, Miyagi 9808578 Japan, and [⊥]Francis Bitter Magnet Laboratory, [¶]Department of Electrical Engineering and Computer Science, and [#]Department of Physics, Massachusetts Institute of Technology, Cambridge, Massachusetts 02139-4037, United States

ABSTRACT Bernal (ABA stacking order) and rhombohedral (ABC) trilayer graphene (3LG) are characterized by Raman spectroscopy. From a systematic experimental and theoretical analysis of the Raman modes in both of these 3LGs, we show that the G band, G′ (2D) band, and the intermediate-frequency combination modes of 3LGs are sensitive to the stacking order of 3LG. The phonon wavevector q, that gives the double resonance Raman spectra is larger in ABC than ABA, which is the reason why we get the different Raman frequencies and their spectral widths for ABA and ABC 3LG. The weak electron−phonon interaction in ABC-stacked 3LG and the localized strain at the boundary between ABC- and ABA-stacked domains are clearly reflected by the softening of the G mode and the G′ mode, respectively.

KEYWORDS: graphene · Raman scattering · stacking order · electron−phonon interaction · double resonance Raman spectroscopy

After a few years of intensive study on single layer and bilayer graphene (1LG, 2LG), many exceptional, fundamental, and promising practical properties of such two-dimensional carbon materials have been revealed.[1−3] Most recently, trilayer graphene (3LG) becomes an active focus.[4−9] For the natural structure, the most stable 3LG possesses a Bernal (ABA) structure, where the first two layers show honeycomb lattice stacking just as in the AB Bernal bilayer with the A-atoms in the second layer right above the A-atoms in the first layer and the B-atoms in the second layer are above the centers of the hexagons of the first layer, while the A and B carbon atoms in the third layer occupy exactly the same in-plane locations as the atoms in the first layer, as shown in Figure 1a. On the other hand, a metastable phase of 3LG, which is in fact quite stable in the sense of being unchanged even after an annealing process at 800 °C,[10] exists with a rhombohedral (ABC) structure. In the ABC stacking arrangement of 3LG, when the third layer is stacked, the carbon atoms in the third layer are located in such a way that the pairs of A-atoms in the first two layers are located over the centers of the hexagons of the third layer, as shown in Figure 1b.

The electronic band structures of 2LG and 3LG differ remarkably from that of monolayer graphene because of the interlayer coupling. This coupling is usually featured by the transfer energies between the nearest neighbor carbons stacked above each other on two adjacent layers being denoted by γ_1, while the further-neighbors have transfer energies γ_3 and γ_4.[11] Hence, the stacking order and the resulting relative positions of carbon atoms in each layer could crucially influence both the transfer energies and the electronic properties, especially in the energy region near the Dirac point. Though there are only a few reports in the literature, the effects of the ABA and ABC stacking sequence on some of the electronic properties of 3LG have been demonstrated both theoretically and experimentally.[5,11−14] The most recent and interesting experimental finding is the dependence of the electrical transport properties on the stacking order.[8] In the integer quantum Hall effect (IQHE) measurements,[8] the ABC-stacked 3LG presents a new plateau sequence in contrast to that for the ABA-stacked 3LG: missing some Hall plateaus at filling factors like $\nu = 8$ and $\nu = 12$, which is a monolayer-like behavior. This is mainly because of the so-called superefficient screening effect[12] since the ABC-stacked 3LG is less sensitive than ABA-stacked 3LG to the voltages across layers, usually induced by applying a gate voltage. In contrast to the ABC-stacked 3LG, the gate voltage and the induced charge redistribution in the ABA-stacked 3LG could easily break the lattice inversion symmetry and consequently introduce a difference to the Landau levels originating from the valleys at

* Address correspondence to yuting@ntu.edu.sg.

Received for review July 18, 2011 and accepted October 1, 2011.

Published online October 01, 2011
10.1021/nn203472f

K and K′. The contrasting plateau sequences for rhombohedral ABC-stacked and Bernal ABA-stacked 3LG make the IQHE an effective way to identify the stacking order of 3LG.[8] Another relatively simple yet reliable approach to identify the stacking order is infrared (IR) absorption spectroscopy or optical conductivity spectroscopy.[10,15] The different crystallographic symmetry of the rhombohedral graphene layers compared with that of the Bernal graphene layers results in the extreme of the energy bands shifting away from the *K* point,[10,15,16] which causes a relative shift of the optical absorption peak. Though IR spectroscopy could remove many critical requirements for performing IQHE measurements, such as the complicated processes for device fabrication, low temperatures and high magnetic fields, specialized instruments are still needed. Further, it is very hard for IR spectroscopy to reach submicrometer spatial resolution. Confocal micro-Raman mapping and spectroscopy which have several advantages, such as relatively high spatial resolution (a few hundreds of nanometer), high spectral efficiency (tens of milliseconds integration time for a clear spectrum), and no special sample preparation, might be able to solve the issues for IQHE or IR. In fact, Raman imaging and spectroscopy have already been shown to provide useful tools for studying many properties of graphene, such as the electronic structure,[17−19] electron−phonon interaction,[20,21] life times of phonons,[22] phonon dispersion relations,[23] crystal orientation,[24,25] doping level,[26,27] defects,[28,29] edge chirality,[30,31] strain,[32,33] and mechanical properties.[34] Most recently, Rao *et al.*[35] and our group both[36] demonstrated for AB-stacked bilayer graphene that the appearance of the M band located at around 1750 cm^{-1} strictly depends on the AB stacking order, which can be used for characterizing bilayer graphene. Furthermore, Lui and his coworkers show that the G′ (also called 2D) spectral width could be employed to identify the stacking sequence of 3LG and tetralayer graphene (4LG).[10] However, as indicated by them and by us, the G′ mode width is sensitive to the electrical environment, disorder, and strain. Thus the identification of the stacking order by monitoring only the G′ mode width is not sufficient in distinguishing between ABA and ABC stacked graphene.

In this work, we propose that the G mode and the newly assigned weak peaks appearing in the intermediate frequency region (1690−2150 cm^{-1}) can be used for identifying ABA and ABC 3LG. In particular, (1) the combination modes of the longitudinal optic (LO) mode and the out-of-plane breathing mode (ZO) denoted here by LOZO, (2) the overtone modes of the out-of-plane tangential optic (oTO) mode denoted by 2oTO,[36] and (3) the G mode are all sensitive to the stacking order of 3LG. To identify the stacking order, not only the peak positions of these modes as a function of the laser excitation energy, but also their spectral widths, can be used consistently. It is not easy to assign the phonon modes in the intermediate frequency region by using two laser energies without using the information coming from theory, since there are many weak peaks in this spectral region and since some combination phonon modes change their relative positions in the Raman spectra with increasing laser excitation energy, which can be understood by the double resonance Raman theory.[37,38] Our findings demonstrate that Raman mapping and spectroscopy provide consistent, reproducible, and sensitive approaches for characterizing the stacking order, once we know the frequency, linewidths, and phonon identification of weak, stacking-order-specific Raman peaks in 2LG and 3LG.

In the next section, we first explain how to select ABA and ABC regions of 3LG by Raman spectra. Then we show the intermediate Raman spectra for ABA and ABC regions. After that, we briefly explain the method of calculation and the double resonance Raman theory for the combination modes and then the calculated results of the 2oTO and LOZO Raman spectra are given. Further, we will assign the observed Raman peaks of 2OTO and LOZO combined with the calculated results. Subsequently, we will discuss the other combination modes of iTOLA and LOLA modes and explain the origin of G and G′ mode spectra width for ABA and ABC. Finally, we discuss the effect of local strain on G and G′ modes.

RESULTS AND DISCUSSION

Selection of the ABA and ABC Regions of 3LG from the Raman Mapping. The Raman G mode intensity (for undoped graphene samples) and the Raman G′ mode width (for Bernal stacked graphene samples) have been widely used[39−42] for the characterization of the numbers of graphene layers, along with optical approaches, such as optical images, contrast spectroscopy/imaging and optical transmittance. Figure 1 panels c−e present the optical contrast and G mode intensity images of a mechanically exfoliated graphene sheet. The homogeneous contrast of these images clearly shows that the sample thickness or the number of graphene layers is identical over almost the entire sheet. For example, the images also show a narrow strip of 2LG and a small triangle of a thicker part at the left edge and corner, respectively, which show a different contrast. It can be determined from the contrast and Raman spectra (not shown here) that the dominant part of the sample is 3LG. The width of the G′ mode shown in Figure 1f also supports this conclusion. When we make an image map for the spectral width for the G′ band over 40−68 cm^{-1}, the image of the G′ bandwidth in the 3LG region exhibits two parts with strikingly different contrasts, indicating the existence of two domains with different stacking orders. Using double resonance Raman theory (see Results and Discussion (5)), we can

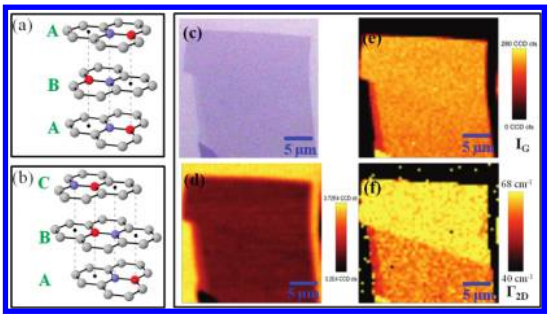

Figure 1. (a,b) Stacking structures of 3LG with (a) ABA and (b) ABC stacking sequences. The two atoms in one unit cell are shown with special shadings. (c) Optical and (d) contrast images of a 3LG sheet. Raman images of (e) the G mode intensity and (f) the G′ mode width of the 3LG sheet taken at E_{laser} = 2.33 eV. The intensity and width scales that were used are shown on the right. Note: A small piece of thick graphite exists at the lower left corner of the sample.

assign the brighter (broader G′ mode) part as ABC-stacked 3LG, while the darker (narrower G′ mode) past is assigned as ABA-stacked 3LG which is consistent with the previous results.[10] The stacking sequences of these two domains are further confirmed by the IR measurement (see Supporting Information: Figure S1), where the feature peaks of ABC- and ABA-stacked 3LG are consistent, too, with the previous measurements of the optical conductivity spectra.[10] For the specified regions of ABA and ABC, we investigate Raman spectra and widths observed by confocal Raman spectroscopy which are directly compared with the calculated results of Raman spectra.

Raman Spectra in the Intermediate Frequency Range. First we focus our attention on weak Raman peaks in the intermediate frequency range (1690−2150 cm^{-1}). Recently, we found weak Raman modes in the intermediate frequency range (1690−2150 cm^{-1}) in Bernal stacked 2LG and few-layer graphene.[36,43] Especially, the M bands (1690−1800 cm^{-1}) could be used as a fingerprint of the AB-stacked 2LG since the M bands are absent for the 2LG without stacking order. In Figure 2, we show Raman spectra in the range of 1690−2150 cm^{-1} for the ABC and ABA 3LG regions. The magnified views of the Raman spectra in the M band range, including fitting curves for ABA- and ABC-stacked 3LG, are shown in Supporting Information, Figure S2. The positions (and full widths at the half-maximum fwhm intensity) of each peak are labeled as 1740 (16) in cm^{-1} in Figure S2.

Method of Calculation and Double Resonance Raman Theory. To assign the Raman peaks in the range from 1690 to 1800 cm^{-1}, we have calculated the Raman intensity of ABA- and ABC-stacked 3LG for possible phonon combination modes, using the double resonance Raman theory for graphite. The calculation method is described in a previous paper for bilayer graphene.[43] In short, the phonon frequency and eigenvectors are calculated by using the force constant parameters proposed by Furukawa for the in-plane phonon

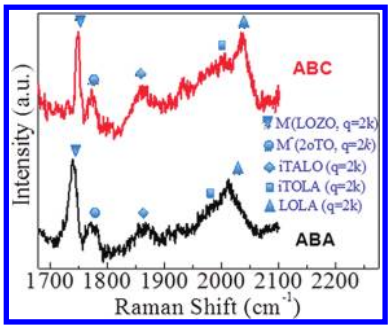

Figure 2. Raman spectra of the intermediate frequency modes in the 1690−2150 cm^{-1} range taken at E_{laser} = 2.33 eV for ABC-stacked and ABA-stacked 3LG domains and their identification.

TABLE 1. The Out-of-Plane Force Constants Used for Trilayer Graphene. The Units Are 10^4 dyn/cm

neighbor	first	second	third	fourth
radial	0.27469	0.059552	−0.047388	0.1890
tangential	−0.59341	0.36712	0.004739	−0.068628

modes[43,44] and the force constant parameters shown in Table 1 for the out-of-plane phonon modes. To obtain consistency between the two sets of force constant parameters, we use the force constant sum rule $\Sigma_{(n=1,2,3,4)}\ j_n\phi^{(n)}r_i^2 = 0$.[44] Here, j_n is number of carbon atoms, $\phi^{(n)}$ is a force constant parameter in the nth neighbor shell, and r_i is the distance between the central and the ith carbon atom.[45,46]

Figure 3 shows five different "optical", out-of-plane phonon modes for ABA- ((a−e)) and ABC- ((f−j)) stacked 3LG at the Γ point in the two-dimensional Brillouin zone (2D BZ) of graphene. Figure 3 modes a/f and b/g are two out-of-plane breathing modes, ZO and ZO′, respectively, while Figure 3 modes c−e/h−j are the three out-of-plane transverse optical (oTO) modes. It is noted that the ZO (ZO′) modes do not exist for 1LG, and that the oTO mode is not a Raman active mode for 1LG. In the case of 2LG (3LG), we have one (two) ZO and two (three) oTO modes, which are all Raman active modes. As is shown in Figure 3, the differences of the frequencies for each phonon mode between ABA and ABC are very small (0.2 cm^{-1} at most) because the interlayer force constant for a next nearest neighbor layer is tiny. Thus we cannot distinguish the staging order from one-phonon Raman spectroscopy. However, using the double resonance Raman signal, we can distinguish the staging order as discussed below.

Since there are no combination or overtone modes that are associated with phonons near the K point of the 2D BZ in the intermediate frequency region, we consider only the intravalley double resonance Raman scattering process. There are two possibilities for two-phonon Raman modes, that is (1) the overtones of the oTO (Figure 3(c−e) and (h−j)) phonon modes (2oTO), and (2) the combination modes of the longitudinal

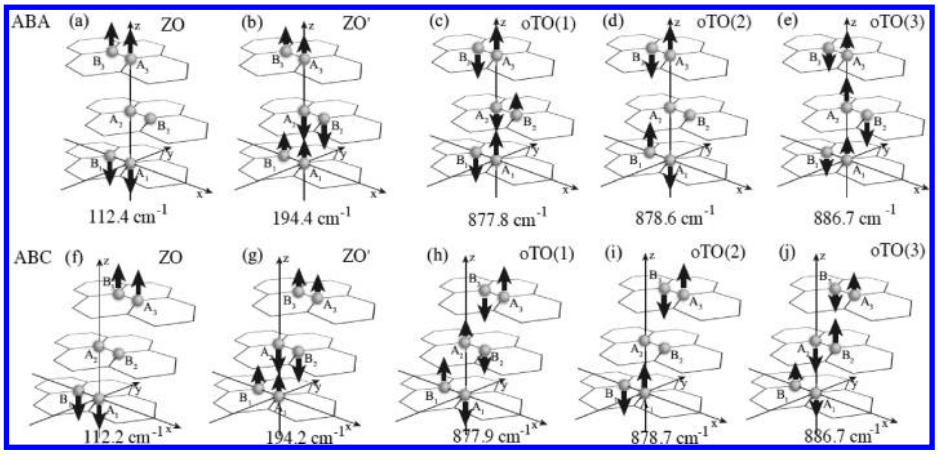

Figure 3. Five Different Optical Out-of-Plane Phonon Modes of ABA- (a−e) and ABC- (f−j) Stacked Trilayer Graphene at the Γ Point (q = 0).

optical (LO) and the out-of-plane breathing (ZO) (Figure 3a,f) phonon modes (LOZO), which appear around 1700−1800 cm^{-1}. As shown in Figure 3, since the differences of the ZO and oTO phonon frequencies for the two stackings are all small at the Γ point, the differences of the 2oTO and LOZO frequencies between ABA and ABC for a general phonon wavevector q are small (within several cm^{-1}). This does *not* however mean that we cannot distinguish between the Raman spectra of ABA and ABC stacked 3LG. Here we use the fact relevant to the double resonance condition for the phonon wavector q that either $q = 0$ or $q = 2k$ (k is the momentum of the photoexcited electron measured from the K point) are selected as the dominant wave vectors for the double resonance Raman spectra.[36,37] Especially for the case of $q = 2k$, the phonon wavevector q increases with increasing laser energy (E_{laser}). Therefore the phonon frequency shows a dispersive behavior by changing E_{laser}, which we can use for the phonon assignment of the dispersive Raman peaks ($q = 2k$) and the nondispersive Raman peaks ($q = 0$). Further, since the k values are different for the different electronic energy bands of ABA- and ABC-stacked 3LG for a given E_{laser},[47] the corresponding q and phonon frequencies appear at a non-negligible difference frequency, which we use as a major factor in finding the identification of the stacking-order-dependent Raman peaks.

Calculated Results of the 2oTO and LOZO Spectra. Figure 4a shows the calculated Raman shifts of the 2oTO (overtones of the oTO) and LOZO (the combination mode of the LO and ZO vibration) peaks as a function of E_{laser} from 1.6 to 2.8 eV. Black circles and red crosses are for the ABA- and ABC-stacked 3LG, respectively. It is clear that there is no significant difference in the phonon frequencies of the 2oTOs (or LOZOs) for ABA- and ABC-stacked 3LG, since the interlayer interaction force constant is sufficiently small. The nondispersive (q = 0) 2oTO (3) peaks around 1755 cm^{-1} correspond to the M^{+} peaks of ABC- and ABA-stacked 3LG in Figure 2 whose frequencies do not change by changing E_{laser}. We expect relatively weak ($q = 0$) 2oTO (1) and (2) peaks around 1755 cm^{-1} from the calculation which are not clearly seen in the experiment. The dispersive ($q = 2k$) LOZO and 2oTO (1−3) peaks correspond to M^{-} peaks which are different between ABA and ABC for a given E_{laser}, as shown in Figure 2.

Since the dispersive ($q = 2k$) 2oTO (1,2) and (3) peaks intersect with the LOZO peak at around E_{laser} = 2.1 and 2.4 eV as shown in Figure 4a, the assignment of these peaks in this E_{laser} range is difficult only from an experimental viewpoint. We expect that the intersection of the two phonon modes affects both the peak intensities and the widths of the LOZO peak at the crossing points. These phenomena appear in the experimental M^{-} peaks in Figure 2. In fact, we observe one broad M^{-} peak for ABA-stacked 3LG, while there are two M^{-} peaks for ABC-stacked 3LG.

Figure 4 panels b and c show, respectively, the calculated Raman intensities of the 2oTO for ABA- (Figure 3c−e) and the 2oTO for ABC- (Figure 3h−j) stacked 3LG at E_{laser} = 2.33 eV. Black, red, and blue lines denote 2oTO(1) (Figure 3 mode c or h), 2oTO(2) (Figure 3 mode d or i), and 2oTO(3) (Figure 3 mode e or j), respectively. Since the phonon amplitudes of the carbon atoms in the unit cell in Figure 3 are different for different graphene layers, a local relative volume change of 3LG is associated with these oTO phonons. Thus the electron−phonon matrix elements of all oTO phonons have nonzero values in the double resonance Raman scattering process. In Figure 4b, the local volume change of the oTO (3) phonon (Figure 3e), which is relevant to the deformation potential (that is the electron−phonon interaction), is slightly larger than that of oTO (1) and (2) (Figure 3c,d). Thus the calculated intensity of the 2oTO (3) is higher than that of the other overtone modes (black and red lines). On the other hand, in the case of ABC stacking (Figure 4c), the calculated intensity of the oTO(1) and (2) phonons (Figure 3h,i) is higher than that of the oTO (3) phonon

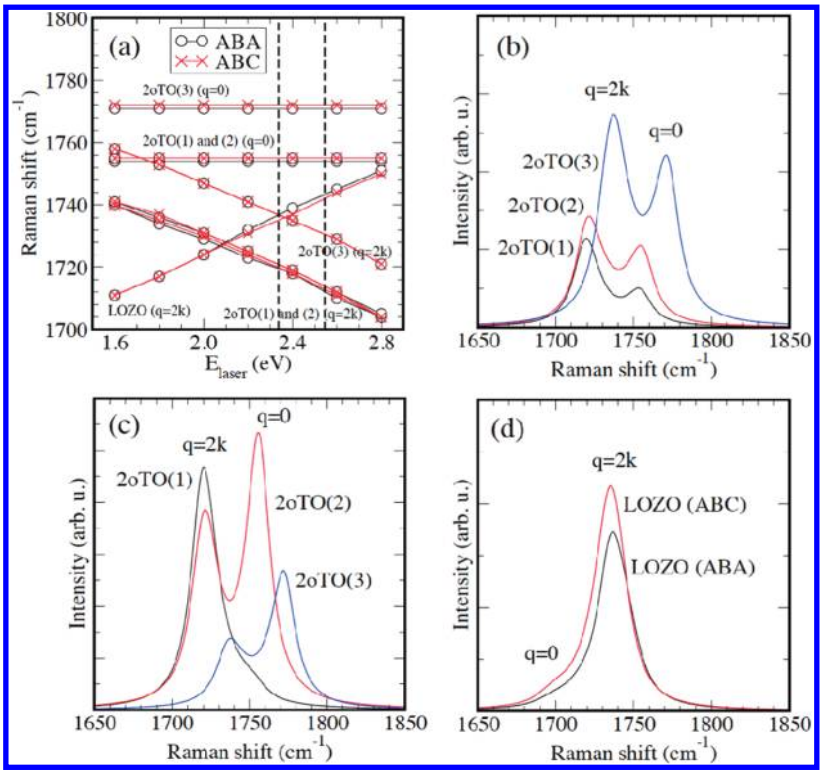

Figure 4. (a) The calculated Raman shifts of the 2oTO and LOZO peaks as a function of E_{laser}. Black circles (red crosses) are for ABA- (ABC-) stacked 3LG. (b) The calculated Raman intensity of the 2oTO modes for ABA-stacked 3LG. Black, red, and blue lines correspond to Figure 3 oTO modes c, d, and e, respectively. (c) The calculated Raman intensity of the 2oTO modes for ABC stacking. Black, red and blue lines correspond to Figure 3 oTO modes h, i, and j, respectively. (d) The calculated Raman intensity of the LOZO mode for ABA (black line) and ABC (red line) stacking. For panels b–d, we used E_{laser} = 2.33 eV for the calculations.

(Figure 3j) because of the local volume change of these phonons. Figure 4d shows the calculated Raman intensity of the LOZO mode for ABA- (black line) and ABC- (red line) stacked 3LG at E_{laser} = 2.33 eV. The calculated intensities of the LOZO mode are similar to each other between the ABA- and ABC-stacked 3LG. Thus we consider that, in this work, the oTO (3) for ABA and the oTO (1) and (2) for ABC (Figure 3e,h,i) contribute most sensitively to the difference in the M^- peak width between ABA- and ABC-stacked 3LG.

Assignment of 2oTO and LOZO Modes. To assign the modes in this M band range, the Raman spectra of ABC-stacked 3LG obtained at E_{laser} = 2.54 and 2.33 eV are plotted together in Supporting Information, Figure S3. Comparing the experimental data to our theoretical calculation (Figure 4a), the peak at 1748 cm^{-1} (obtained E_{laser} = 2.33 eV) is assigned as the LOZO (M^-) mode as it presents a positive dispersion, while the peak at 1774 cm^{-1} (obtained for E_{laser} = 2.33 eV) is assigned to the 2oTO (q = 0) (M^+) mode. The M^+ peak contains two 2oTO (q = 0) peaks. Since the Raman intensity of the 2oTO feature decreases with increasing E_{laser}, the intensity of the higher energy 2oTO(3) (q = 0) peak becomes weak at E_{laser} = 2.54 eV. Thus the width of the M^+ peak becomes narrow at E_{laser} = 2.54 eV. The calculated energy difference between the higher 2oTO(3) and lower 2oTO(1,2) (q = 0) peaks is large (20 cm^{-1}) compared with the experimental results (11 cm^{-1} for ABA and 7 cm^{-1} for ABC). This difference may come from our selection of force constant parameters for calculating the interlayer interaction and the detailed discussion of this difference between experiment and theoretical prediction remains for future study. The 1730 cm^{-1} peak at E_{laser} = 2.33 eV corresponds to the lower energy 2oTO(1) and (2) (q = 2k) peak. According to Figure 4a, we expect that there is a higher 2oTO(3) (q = 2k) peak around the M^- band (LOZO) for E_{laser} = 2.33 eV. Since 2oTO (q = 2k) has a negative dispersion, the 1732 cm^{-1} peak at E_{laser} = 2.54 eV corresponds to the higher 2oTO(3) (q = 2k) peak. The calculated Raman shift at 1740 cm^{-1} of M^- (LOZO) for ABC-stacked 3LG is 10 cm^{-1} smaller than the experimental value of M^- (1750 cm^{-1}) in Figure 2. Even though there is a difference between the calculated phonon frequency and the experimental results, we can assign each peak by comparing the relative positions of the various peaks.

iTOLA and LOLA Combination Modes. It is worth noting that some of the combination modes in this intermediate frequency range such as iTO+LA (1990 cm^{-1}) and LO+LA (2030 cm^{-1}) are blueshifted in the ABC-stacked 3LG relative to ABA-stacked 3LG (1980 cm^{-1}, 2020 cm^{-1}). These differences in the frequency may be because the q values of the phonons required to

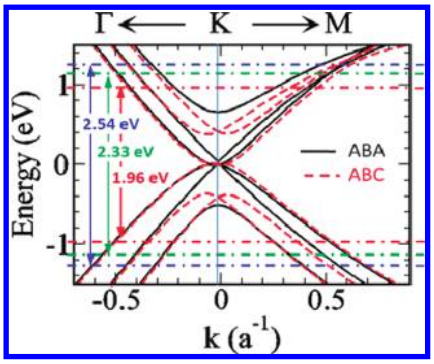

Figure 5. Electronic band structures E(k) of ABA- and ABC-stacked 3LG in the low energy range and near the K point in the Brillouin zone. The excitation lasers used are also indicated, together with the red, green, and blue color of their light emissions.

satisfy the double resonance scattering process are different for ABC- and ABA-stacked 3LG as shown in Figure 5.

In Figure 5, we show the electronic structures of ABA- and ABC-stacked 3LG by solid and dashed lines, respectively, near the K point in the 2D BZ. As shown in Figure 5, in the energy range covered by the excitation lasers used in our experimental studies, the most significant deviation of the electronic energy bands occurs among the branches along the K–M direction (involving the so-called inner phonon scattering process[48]) and the lower energy level, where the largest differences in the electronic band structures are found. For a given E_{laser}, we always get a larger double resonance q wavevector for ABC stacking. Thus for a phonon mode with a positive phonon dispersion from the Γ point, such as the LO and ZO modes, we get higher double resonance phonon frequencies, while for the weak negative phonon dispersion, we get lower double resonance phonon frequencies. Thus the iTO+LA (q = 2k, 1990 cm^{-1}) and LO+LA (q = 2k, 2030 cm^{-1}) modes can be good phonon modes for use in specifying the ABC stacking order. Since the phonon dispersion is not so steep for the oTO phonon mode, the redshift of the 2oTO mode is not clearly observed. From Figure 3 we expect to see that the more obvious differences in the Raman spectra occur for the subpeaks observed for the higher energy peak. Such a difference shows a greater slope as emphasized by the remarkable behavior for the G′ mode obtained at the lowest E_{laser} (1.96 eV in this work). It is stressed again that this difference in the phonon frequency does not come from the difference in the dispersion between ABA and ABC stacking, but rather from the difference in the electronic energy dispersion and in the q values.

Spectral Widths of the G and G′ Modes. Now we discuss the difference in the spectral widths of the G-band for the ABA and ABC stacking orders. Figure 6 shows the Raman spectra of the G mode from the ABC- and ABA-stacked domains shown in Figure 1f. From Figure 6, we

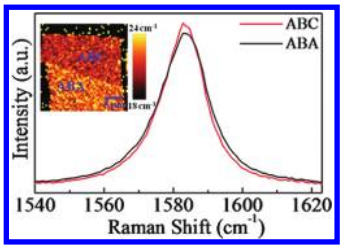

Figure 6. Raman spectra of the G mode for ABC- and ABA-stacked trilayer graphene domains taken at E_{laser} = 2.33 eV. The inset shows the Raman image of the G mode width of the trilayer graphene where the ABC- and ABA-stacked 3LG regions are identified.

can say that the G mode of the ABC-stacked 3LG has a relatively narrower spectral width than that of ABA-stacked 3LG. To check whether this narrowing is a universal feature or not, we performed Raman mapping over the entire sheet shown in the inset of Figure 6. By fitting the G band spectra recorded from point to point (steps = 0.5 μm) with a single Lorentzian peak and extracting the fwhm intensity, we display the G mode width image of the same 3LG sheet (inset of Figure 6). Two areas appear with a remarkably distinct contrast if we take the window of values of the fwhm from 18 to 24 cm^{-1}. It is noted that the shape and dimensions of these two areas perfectly match the domains reflected in the G′ width image (Figure 1f). In the case of the G mode, the ABC-stacked domain exhibits a narrower width while the ABA-stacked domain presents a broader peak, which is the opposite to the case of the G′ band. The narrowing of the G mode in ABC-stacked 3LG could be attributed to the weaker electron–phonon interaction for ABC and thus to the increase of the lifetime of the G phonon as is known to occur for the Kohn anomaly effect.[45]

In Figure 7 we list the images obtained from 2LG to 4LG by showing the corresponding (a) optical image and, (b) G band intensity, from which we can determine the number of graphene layers, and then we show in panel c the fwhm of the G′ band and in panel d the fwhm of the G band, from which we can distinguish between the ABC- and ABA-stacking ordered domains. The one-to-one correspondence between the G′ and G mode width images demonstrates that both of these modes could be used as a convenient and reliable basis for identifying the stacking orders. Furthermore, analysis of the intermediate frequency modes, as well as the G and G′ modes, of course, could distinguish between ABC and ABA stacking orders much more convincingly, when considered all together with careful observation of the fitted peak positions of the G mode. The small redshift of the G mode for ABC-stacked 3LG relative to its ABA counterpart can be observed, and such a small shift is sufficient to produce a noticeable contrast in the Raman images of the G mode position, as can be seen in Supporting Information, Figure S4. The slight softening of the G mode

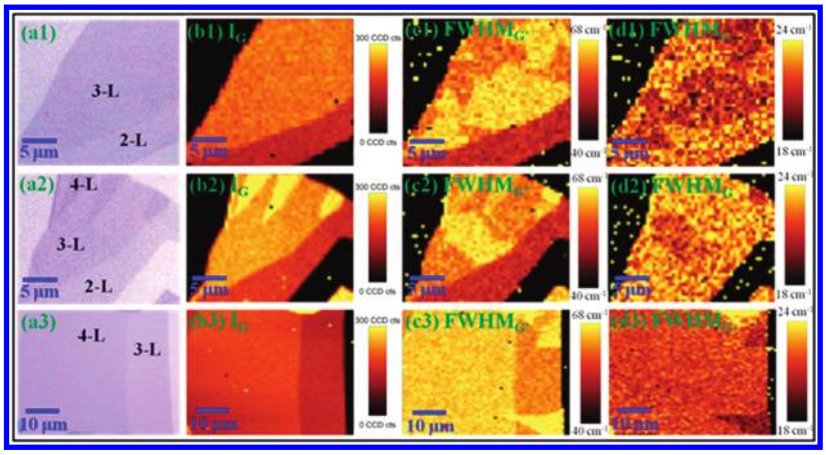

Figure 7. (a1−a3) Optical images of three graphene sheets consisting of 2LG, 3LG, tri- and tetra-layers. Panels b1−b3, c1−c3, and d1−d3 are Raman images of the G mode intensity, the G′ mode width, and the G mode width of the corresponding areas shown in panels a1−a3, respectively. The excitation energy here is E_{laser} = 2.33 eV.

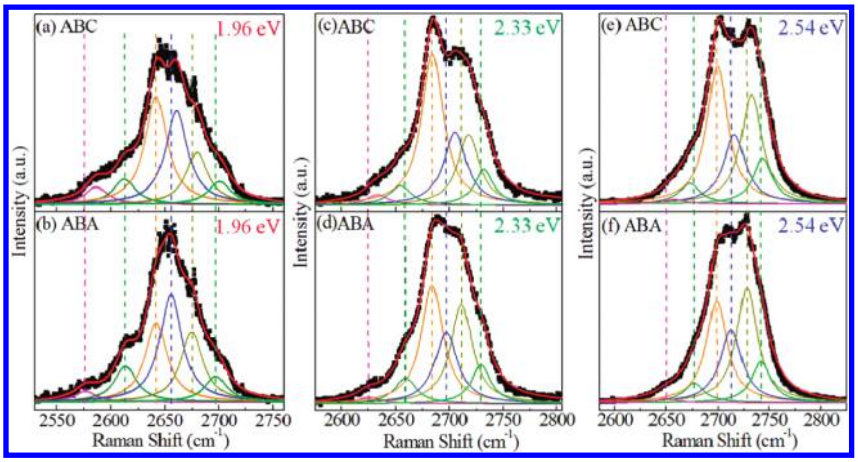

Figure 8. Raman spectra of the G′ modes of ABC- and ABA-stacked 3LG taken at E_{laser} = 1.96, 2.33, and 2.54 eV. The vertical dashed lines indicate the positions of the subpeaks of the G′ mode in ABA-stacked 3LG. The blueshifts of the higher frequency subpeaks of ABC-stacked 3LG can be clearly seen.

frequency for the ABC-stacked 3LG is likely due to the small difference between the phonon band structures of the ABC- and ABA-stacked 3LG.[10,49]

Figure 8 presents the G′ modes of ABA- and ABC-stacked 3LG obtained using the three excitation energies of 1.96, 2.33, and 2.54 eV, together with the fitting curves. As shown, the G′ mode is fitted by six Lorentzian peaks (peak width = 25 cm^{-1}). The clear blueshifts of the subpeaks, especially those of higher frequencies for the ABC-stacked 3LG provide direct evidence of our hypothesis. The changes of the relative intensities of these six subpeaks between the ABA- and ABC-stacked 3LG will also affect the fwhm of the G′ mode so that a more detailed analysis of this feature remains for future investigation.

The Effect of Local Strain on the G and G′ Modes. Interestingly, in one of the 3LG samples (see Figure 1), localized strain is observed at the boundary between two differently stacked domains. Supporting Information, Figure S6 panels a and b, respectively, show the Raman images of the G′ and G mode positions in such a boundary region. The dark stripes located at the boundary between the two domains indicate a redshift or a frequency softening of both the G′ and G modes. To further exploit this redshift, a Raman line scan across the boundary, as denoted by the green arrows in the insets of Supporting Information Figure S6c,d was performed. The fitted spectral parameters, namely the G′ (G) widths and G′ (G) peak positions, are plotted as a function of their spatial locations across the boundary, as shown in Figure S6 panels c and d, respectively.

As indicated by their Raman spectra and images (see Figure 1f and Figure 6), the ABC-stacked 3LG regions show a larger G′ bandwidth and a smaller G bandwidth than the ABA-stacked 3LG. A slight redshift of the G mode for ABC-stacked 3LG could also be observed in the line scan plot of the G mode frequency (Figure S6d). Both the G′ and G modes show an obvious dip in the plots of their peak positions. The maximum shift of the G′ mode is roughly twice that of the G mode, a typical feature of the expected tensile strain-induced softening of the G′ and G phonons.[24,25,32,33] Considering the way

the third layer is stacked and the different resulting locations of the carbon atoms, we believe that a lattice mismatch should exist between the ABC- and ABA-stacked regions and should result in a tensile strain that is localized at the boundary between these two stacked regions. A simple calculation made by considering the lattices of the ABC- and ABA-3LGs, especially for the third layer and the dimensions of the boundary obtained from the dip in the plot of the G′ mode positions, estimates that the strain here is around 0.1%, which provides a fairly good fit to our Raman observations of a redshift of 5−6 cm^{-1} for the G′ mode (Figure S6c).[50] The existence of the localized strain at the boundary between ABC- and ABA-stacked few layer graphene might be able to further enrich the study of stacking order-dependent electronic properties of few layer graphene, which will be another topic for future work.

CONCLUSION

We have studied the Raman modes of ABC- (rhombohedral) and ABA-stacked (Bernal) 3LG. Our results successfully demonstrate that, by monitoring at the same time the G and G′ modes and the intermediate frequency modes (2oTO, LOZO, iTOLA, and LOLA from 1690 to 2150 cm^{-1}), their Raman spectra and their Raman images could together provide convenient and reliable approaches for identifying the regions of samples with ABC and ABA stacking order and allow visualization of the shape, location, and dimensions of the domains with different layer stacking sequences. The observation of localized strain at the boundary between the ABC- and ABA-stacked domains calls for further Raman and transport studies of such an interesting and important system as few layer graphene with different stacking orders.

EXPERIMENTAL METHODS

In this work, the graphene layers were prepared by the mechanical cleavage of natural graphite and transferred onto a 300 nm SiO_2/Si substrate. An optical microscope was used to locate the thin layers, and the number of layers was further identified by white light contrast spectra, and by the absolute Raman intensity of the G mode.[39] The stacking sequence was then determined by IR spectroscopy and the width of the Raman G′ mode. The IR measurements were carried out in the reflection setup using a micro-Fourier transform IR spectrometer with a mercury cadmium telluride (MCT) detector. The white light contrast spectra were acquired using a WITec CRM200 Raman system with a 150 lines/mm grating. The Raman spectra were obtained using a WITec CRM200 Raman system with a 600 lines/mm grating and using 488 nm (E_{laser} = 2.54 eV), 532 nm (E_{laser} = 2.33 eV), and 633 nm (E_{laser} = 1.96 eV) laser excitation. To compare the effects of the grating lines, a 1800 lines/mm grating was also used for single spectrum measurement. The laser power was kept below 0.1 mW on the sample surface to avoid laser-induced heating.

Acknowledgment. This work is supported by the Singapore National Research Foundation under NRF RF Award No. NRF-RF2010-07 and MOE Tier 2 MOE2009-T2-1-037. R. Saito acknowledges MEXT Grant (No. 20241023). M. S. and G. Dresselhaus acknowledge NSF/DMR 10-04147. T. Yu gives thanks for the valuable discussions with Professor Young-Woo Son. C. X. Cong thanks Mr. Chow Wai Leong for his help on Raman measurements. J. Shang thanks Professor Cesare Soci for his help with the IR measurements.

Supporting Information Available: The following results are shown as the supporting figures: (1) optical conductivities vs photon energy of ABC- and ABA-stacked 3LG; (2) Raman spectra of ABC-stacked and ABA-stacked 3LG in the M band spectral range obtained at E_{laser} = 2.33 eV; (3) Raman spectra of ABC-stacked 3LG in the M band spectral range obtained at 2.54 and 2.33 eV; (4) Raman images of the G mode position of three different graphene sheets; (5) optical image of a tetralayer graphene sheet with a small portion of pentalayer, Raman images of the G′ mode width and of the G mode width of the tetralayer graphene sheet; (6) Raman images of the G′ band position and the G band position, Raman line scan of the G′ bandwidth and position, and the G bandwidth and position crossing the boundary of the ABC- and ABA-stacked domains. This material is available free of charge *via* the Internet at http://pubs.acs.org.

REFERENCES AND NOTES

1. Castro Neto, A. H.; Guinea, F.; Peres, N. M. R.; Novoselov, K. S.; Geim, A. K. The Electronic Properties of Graphene. *Rev. Mod. Phys.* **2009**, *81*, 109–162.
2. Chakraborty, T.; Abergel, D. A., D. S. L.; Apalkov, V.; Berashevich, J.; Ziegler, K. Properties of Graphene: A Theoretical Perspective. *Adv. Phys.* **2010**, *59*, 261–482.
3. Wu, Y. H.; Yu, T.; Shen, Z. X. Two-Dimensional Carbon Nanostructures: Fundamental Properties, Synthesis, Characterization, and Potential Applications. *J. Appl. Phys.* **2010**, *108*, 071301-1–071301-38.
4. Zhang, F.; Sahu, B.; Min, H. K.; MacDonald, A. H. Band Structure of Abc-Stacked Graphene Trilayers. *Phys. Rev. B* **2010**, *82*, 035409-1–035409-10.
5. Craciun, M. F.; Russo, S.; Yamamoto, M.; Oostinga, J. B.; Morpurgo, A. F.; Thrucha, S. Trilayer Graphene Is a Semimetal with a Gate-Tunable Band Overlap. *Nat. Nanotechnol.* **2009**, *4*, 383–388.
6. Koshino, M.; McCann, E. Gate-Induced Interlayer Asymmetry in ABA-Stacked Trilayer Graphene. *Phys. Rev. B* **2009**, *79*, 125443-1–125443-5.
7. Zhang, L.; Zhang, Y.; Camacho, J.; Khodas, M.; Zaliznyak, I. A. The Experimental Observation of Quantum Hall Effect of *L*=3 Chiral Charge Carriers in Trilayer Graphene. **2011**, arXiv: physics/1103.6023v1. arXiv.org e-Print archive. http://www.arxiv.com/abs/1103.6023 (accessed 15 Apr 2011).
8. Kumar, A.; Escoffier, W.; Poumirol, J. M.; Faugeras, C.; Arovas, D. P.; Fogler, M. M.; Guinea, F.; Russo, S.; Goiran, M.; Raquet, B., Integer Quantum Hall Effect in Trilayer Graphene. **2011**, arXiv: physics/1104.1020v1. arXiv.org e-Print archive. http://arxiv.org/abs/1104.1020 (accessed 15 Apr 2011).
9. Bao, W.; Jing, L.; Lee, Y.; Velasco Jr., Jr.; Kratz, P.; Tran, D.; Standley, B.; Aykol, M.; Cronin, S. B.; Smirnov, D.; *et al.* Stacking-Dependent Band Gap and Quantum Transport in Trilayer Graphene. **2011**, arXiv: physics/1103.6088v1. arXiv.org e-Print archive. http://arxiv.org/abs/1103.6088 (accessed 15 Apr 2011).
10. Lui, C. H.; Li, Z. Q.; Chen, Z. Y.; Klimov, P. V.; Brus, L. E.; Heinz, T. F. Imaging Stacking Order in Few-Layer Graphene. *Nano Lett.* **2011**, *11*, 164–169.
11. Grüneis, A.; Attaccalite, C.; Wirtz, L.; Shiozawa, H.; Saito, R.; Pichler, T.; Rubio, A. Tight-Binding Description of the Quasiparticle Dispersion of Graphite and Few-Layer Graphene. *Phys. Rev. B* **2008**, *78*, 205425−1–205425−16.
12. Koshino, M. Interlayer Screening Effect in Graphene Multilayers with ABA and ABC Stacking. *Phys. Rev. B* **2010**, *81*, 125304−1–125304−7.
13. Latil, S.; Henrard, L. Charge Carriers in Few-Layer Graphene Films. *Phys. Rev. Lett.* **2006**, *97*, 036803−1–036803−4.
14. Avetisyan, A. A.; Partoens, B.; Peeters, F. M. Stacking Order Dependent Electric Field Tuning of the Band Gap in Graphene Multilayers. *Phys. Rev. B* **2010**, *81*, 115432−1–115432−7.

15. Mak, K. F.; Shan, J.; Heinz, T. F. Electronic Structure of Few-Layer Graphene: Experimental Demonstration of Strong Dependence on Stacking Sequence. *Phys. Rev. Lett.* **2010**, *104*, 176404−1–176404−4.
16. Haering, R. R. Band Structure of Rhombohedral Graphite. *Can. J. Phys.* **1958**, *36*, 352–362.
17. Malard, L. M.; Mafra, D. L.; Doorn, S. K.; Pimenta, M. A. Resonance Raman Scattering in Graphene: Probing Phonons and Electrons. *Solid State Commun.* **2009**, *149*, 1136–1139.
18. Malard, L. M.; Nilsson, J.; Mafra, D. L.; Elias, D. C.; Brant, J. C.; Plentz, F.; Alves, E. S.; Neto, A. H. C.; Pimenta, M. A. Electronic Properties of Bilayer Graphene Probed by Resonance Raman Scattering. *Phys. Status Solidi B* **2008**, *245*, 2060–2063.
19. Dresselhaus, M. S.; Malard, L. M.; Pimenta, M. A.; Dresselhaus, G. Raman Spectroscopy in Graphene. *Phys. Rep.* **2009**, *473*, 51–87.
20. Yan, J.; Zhang, Y. B.; Kim, P.; Pinczuk, A. Electric Field Effect Tuning of Electron-Phonon Coupling in Graphene. *Phys. Rev. Lett.* **2007**, *98*, 166802-1–166802-4.
21. Yan, J.; Henriksen, E. A.; Kim, P.; Pinczuk, A. Observation of Anomalous Phonon Softening in Bilayer Graphene. *Phys. Rev. Lett.* **2008**, *101*, 136804-1–136804-4.
22. Kang, K.; Abdula, D.; Cahill, D. G.; Shim, M. Lifetimes of Optical Phonons in Graphene and Graphite by Time-Resolved Incoherent Anti-Stokes Raman Scattering. *Phys. Rev. B* **2010**, *81*, 165405−1–165405−6.
23. Mafra, D. L.; Samsonidze, G.; Malard, L. M.; Elias, D. C.; Brant, J. C.; Plentz, F.; Alves, E. S.; Pimenta, M. A. Determination of La and to Phonon Dispersion Relations of Graphene near the Dirac Point by Double Resonance Raman Scattering. *Phys. Rev. B* **2007**, *76*, 233407-1–233407-4.
24. Huang, M. H., M. Y.; Yan, H. G.; Chen, C. Y.; Song, D. H.; Heinz, T. F.; Hone, J. Phonon Softening and Crystallographic Orientation of Strained Graphene Studied by Raman Spectroscopy. *P. Natl. Acad. Sci. USA* **2009**, *106*, 7304–7308.
25. Mohiuddin, T. M. G.; Lombardo, A.; Nair, R. R.; Bonetti, A.; Savini, G.; Jalil, R.; Bonini, N.; Basko, D. M.; Galiotis, C.; Marzari, N.; *et al*. Uniaxial Strain in Graphene by Raman Spectroscopy: G Peak Splitting, Gruneisen Parameters, and Sample Orientation. *Phys. Rev. B* **2009**, *79*, 205433-1–205433-8.
26. Das, A.; Pisana, S.; Chakraborty, B.; Piscanec, S.; Saha, S. K.; Waghmare, U. V.; Novoselov, K. S.; Krishnamurthy, H. R.; Geim, A. K.; Ferrari, A. C.; *et al*. Monitoring Dopants by Raman Scattering in an Electrochemically Top-Gated Graphene Transistor. *Nat. Nanotechnol.* **2008**, *3*, 210–215.
27. Luo, Z. Q.; Yu, T.; Kim, K. J.; Ni, Z. H.; You, Y. M.; Lim, S.; Shen, Z. X.; Wang, S. Z.; Lin, J. Y. Thickness-Dependent Reversible Hydrogenation of Graphene Layers. *ACS Nano* **2009**, *3*, 1781–1788.
28. Cancado, L. G.; Pimenta, M. A.; Saito, R.; Jorio, A.; Ladeira, L. O.; Grueneis, A.; Souza, A. G.; Dresselhaus, G.; Dresselhaus, M. S. Stokes and Anti-Stokes Double Resonance Raman Scattering in Two-Dimensional Graphite. *Phys. Rev. B* **2002**, *66*, 035415-1–035415-5.
29. Cançado, L. G.; Jorio, A.; Martins Ferreira, E. H.; Stavale, F.; Achete, C. A.; Capaz, R. B.; Moutinho, M. V. O.; Lombardo, A.; Kulmala, T.; Ferrari, A. C. Quantifying Defects in Graphene *via* Raman Spectroscopy at Different Excitation Energies. **2011**, arXiv: physics/1105.0175v2. arXiv.org e-Print archive. http://arxiv.org/abs/1105.0175 (accessed 5 May 2011).
30. You, Y. M.; Ni, Z. H.; Yu, T.; Shen, Z. X. Edge Chirality Determination of Graphene by Raman Spectroscopy. *Appl. Phys. Lett.* **2008**, *93*, 163112-1–163112-3.
31. Cong, C. X.; Yu, T.; Wang, H. M. Raman Study on the G Mode of Graphene for Determination of Edge Orientation. *ACS Nano* **2010**, *4*, 3175–3180.
32. Yu, T.; Ni, Z. H.; Du, C. L.; You, Y. M.; Wang, Y. Y.; Shen, Z. X. Raman Mapping Investigation of Graphene on Transparent Flexible Substrate: The Strain Effect. *J. Phys. Chem. C* **2008**, *112*, 12602–12605.
33. Ni, Z. H.; Yu, T.; Lu, Y. H.; Wang, Y. Y.; Feng, Y. P.; Shen, Z. X. Uniaxial Strain on Graphene: Raman Spectroscopy Study and Band-Gap Opening. *ACS Nano* **2008**, *2*, 2301–2305.
34. Ferralis, N. Probing Mechanical Properties of Graphene with Raman Spectroscopy. *J. Mater. Sci.* **2010**, *45*, 5135–5149.
35. Rao, R.; Podila, R.; Tsuchikawa, R.; Katoch, J.; Tishler, D.; Rao, A. M.; Ishigami, M. Effects of Layer Stacking on the Combination Raman Modes in Graphene. *ACS Nano* **2011**, *5*, 1594–1599.
36. Cong, C. X.; Yu, T.; Saito, R.; Dresselhaus, G. F.; Dresselhaus, M. S. Second-Order Overtone and Combination Raman Modes of Graphene Layers in the Range of 1690−2150 cm^{-1}. *ACS Nano* **2011**, *5*, 1600–1605.
37. Saito, R; Grüneis, A.; Samsonidze, Ge. G.; Brar, V. W.; Dresselhaus, G.; Dresselhaus, M. S.; Jorio, A.; Cançado, L. G.; Fantini, C.; Pimenta, M. A.; Souza Filho, A. G. *New J. Phys.* **2003**, *5*, 157.1–157.15.
38. Saito, R; Jorio, A.; Souza Filho, A. G.; Dresselhaus, G.; Dresselhaus, M. S.; Pimenta, M. A. Probing Phonon Dispersion Relations of Graphite by Double Resonance Raman Scattering. *Phys. Rev. Lett.* **2002**, *88*, 027401-1–027401-4.
39. Ni, Z. H.; Wang, H. M.; Kasim, J.; Fan, H. M.; Yu, T.; Wu, Y. H.; Feng, Y. P; Shen, Z. X. Graphene Thickness Determination Using Reflection and Contrast Spectroscopy. *Nano Lett.* **2007**, *7*, 2758–2763.
40. Graf, D.; Molitor, F.; Ensslin, K.; Stampfer, C.; Jungen, A.; Hierold, C.; Wirtz, L. Spatially Resolved Raman Spectroscopy of Single- and Few-Layer Graphene. *Nano Lett.* **2007**, *7*, 238–242.
41. Ferrari, A. C.; Meyer, J. C.; Scardaci, V.; Casiraghi, C.; Lazzeri, M.; Mauri, F.; Piscanec, S.; Jiang, D.; Novoselov, K. S.; Roth, S.; *et al*. Raman Spectrum of Graphene and Graphene Layers. *Phys. Rev. Lett.* **2006**, *97*, 187401–187401−4.
42. Nair, R. R.; Blake, P.; Grigorenko, A. N.; Novoselov, K. S.; Booth, T. J.; Stauber, T.; Peres, N. M. R.; Geim, A. K. Fine Structure Constant Defines Visual Transparency of Graphene. *Science* **2008**, *320*, 1308–1308.
43. Sato, K.; Park, J. S.; Saito, R.; Cong, C. X.; Yu, T.; Lui, C. H.; Heinz, T. F.; Dresselhaus, G.; Dresselhaus, M. S. Raman Spectra of out-of-Plane Phonons in Bilayer Graphene. *Phys. Rev. B* **2011**, *84*, 035419-1–035419-5.
44. Saito, R.; Furukawa, M.; Dresselhaus, G.; Dresselhaus, M. S. Raman Spectra of Graphene Ribbons. *J. Phys.: Condens. Mater.* **2010**, *22*, 334203-1–334203-6.
45. Gartstein, Y. N. Vibrations of Single-Wall Carbon Nanotubes: Lattice Models and Low-Frequency Dispersion. *Phys. Lett. A* **2004**, *327*, 83–89.
46. Zimmermann, J.; Pavone, P.; Cuniberti, G. Vibrational Modes and Low-Temperature Thermal Properties of Graphene and Carbon Nanotubes: Minimal Force-Constant Model. *Phys. Rev. B* **2008**, *78*, 045410.
47. Aoki, M.; Amawashi, H. Dependence of Band Structures on Stacking and Field in Layered Graphene. *Solid State Commun.* **2007**, *142*, 123–127.
48. Mafra, D. L.; Moujaes, E. A.; Doorn, S. K.; Htoon, H.; Nunes, R. W.; Pimenta, M. A. A Study of Inner Process Double-Resonance Raman Scattering in Bilayer Graphene. *Carbon* **2011**, *49*, 1511–1515.
49. Yan, J. A.; Ruan, W. Y.; Chou, M. Y. Phonon Dispersions and Vibrational Properties of Monolayer, Bilayer, and Trilayer Graphene: Density-Functional Perturbation Theory. *Phys. Rev. B* **2008**, *77*, 125401-1–125401-7.
50. Yoon, D.; Son, Y. -W.; Cheong, H. Strain-Dependent Splitting of the Double-Resonance Raman Scattering Band in Graphene. *Phys. Rev. Lett.* **2011**, *106*, 155502-1–155502-4.